

DIGITAL IMAGE ANALYSIS OF DETERIORATED CONCRETE TREATED WITH URANYL ACETATE FOR DETECTION OF ALKALI AGGREGATE REACTION

Cecilia Olague^{1*}, Gustavo Olague², José A. Pérez³, Eddie Clemente⁴, Gilberto Wenglas⁵, José Castañeda⁶

^{1, 3, 5, 6} Universidad Autónoma de Chihuahua, Facultad de Ingeniería,
Chihuahua, Chih., MÉXICO

^{2, 4} Centro de Investigación Científica y de Educación Superior de Ensenada, Departamento de Ciencias de la Computación, Ensenada, B. C., MÉXICO

Abstract

Despite decades of study of Alkali Aggregate Reaction (AAR), its understanding is complex and its potential prediction is difficult. The AAR detection is made by means of different field and laboratory tests, and once detected its effects are measured. A common AAR tests is the Rapid Identification of Alkali – Silica Reaction Products, which causes that alkali ions contained in the gel AAR become visible as fluorescent and bright areas under ultraviolet illumination. However, these areas do not necessarily show the presence of AAR, as they may appear as a consequence of concrete carbonation or sodium content in the cement paste. This paper present a new method to detect reactive zones in deteriorated concrete samples treated with uranyl acetate using digital images in a computational model of visual attention. The results show the feasibility of identifying more quickly and accurately the presence of zones where AAR occurred in concrete infrastructure.

Keywords: Deteriorated concrete, reactive zones, visual attention, digital images

1 INTRODUCTION

The Alkali-Aggregate Reaction (AAR) is one of the main factors that can be fully or partially responsible for concrete infrastructure deterioration and premature loss of serviceability [1, 2]. Recently, Alkali-Carbonate Reaction (ACR) has been recognized as a different form of Alkali-Silica Reaction (ASR). The ACR involves certain types of dolomite rocks, while the ASR involves various types of silica minerals (SiO₂). ASR is the most common deleterious reaction around the world [3]. The ASR is a chemical reaction in concrete between hydroxyl ions (OH⁻) of the alkalis (Na and K) of the hydraulic cement and certain types of siliceous rocks and minerals such as opal, chalcedony, microcrystalline quartz and glass of volcanic rocks present in some aggregates. This reaction and its product, alkali-silica gel, can under certain circumstances produce concrete swelling and fracturing [4].

Nowadays, the ASR detection and its potential are made by means of different field and laboratory tests, which mostly rely on visual inspections that provide information about the condition of the structure. Nevertheless, the quality of this information depends primarily on the practice and experience of the observer. Few methods have been developed based on computational techniques of digital images analysis.

In this article was described a new and innovative method for detecting quickly and accurately the presence of ASR including reactive aggregates and reaction products. Section 1 describes the basics of the ASR. Section 2 summarizes the work done to date on the topic. Section 3 presents materials and methods. Section 4 summarizes the results of this study. Section 5 presents the discussion of results. Finally, conclusions are presented in Section 6.

2 STATE OF THE ART

Works related to the digital images analysis include those by Garcia del Amo & Calvo [5] in which the presence of ASR was identified through a quartz reaction index (QRI). This study showed that the smaller the size of the quartz grains the higher the specific surface area for the reaction, which increases the ASR magnitude. However, the analysis of other particles different from quartz was not considered. Castro & Wigum [6] conducted a research using petrography through imaging to quantitatively assess the microstructure of aggregates for concrete petrography. The purpose was to demonstrate how digital imaging can be used to overcome some limitations of traditional petrographic method. St'astná et al. [7] conducted a

* Correspondence to: cecilia.olague@gmail.com

research using microscopic techniques combined with image analysis. In this research, the composition of the concrete and its degradation due to ASR were determined. In addition, petrographic characterization of the aggregates was applied. A down size of this research is that it was mainly focused on the identification of aggregates compounded by different types of quartz.

Although the use of computational techniques related to digital image management is not required, one of the tests that are frequently used because it is quick and useful is the Rapid Identification of Alkali Silica Reaction products in Concrete [8] that helps to detect the presence of gel product of the ASR in concrete. This test consists on covering a newly exposed concrete surface with a solution of uranyl acetate followed by observation under ultraviolet light. Uranyl ions replace ions of alkali content in the gel becoming visible as bright fluorescent areas under ultraviolet illumination. However, the problem with this test is that it will not necessarily indicate the presence of the reaction product since it could be due to concrete carbonation.

As mentioned above, it is necessary to develop more flexible and precise methods and techniques to accurately assess the presence of ASR and the extent of internal damage in concrete elements analyzed. The main objective of this research is to develop a computational model that allows the detection and evaluation of potential ASR by detecting reactive zones through computer vision and evolutionary computation applied to concrete samples treated with uranyl acetate. This research includes field sampling, laboratory testing and analysis, image database development, computational model of artificial vision creation, method implementation, and analysis of results. Visual detection techniques applied to ASR deteriorated concrete images treated with uranyl acetate can be effective for prognosis of ASR [9].

3 MATERIALS AND METHODS

In this section the criteria for sampling, the process of obtaining and manipulating images as well as the necessary steps to create the image database required to test the computational model are described. At the end of the same section, alternative standard methods for validation of the results are described.

3.1 Sample Extraction in Portland Cement Concrete Pavements (PCCP)

For sampling location identification samples should be taken in pavement roads built with Portland cement concrete (PCCP). According to Stark (1991) [1] to be considered for sampling a road should show ASR presence to the naked eye. The sampling was conducted in the city of Chihuahua, Chihuahua, Mexico, at the locations showed in Table 1.

TABLE 1: Sampling location.

<i>Identification</i>	<i>Road segment</i>	<i>Construction date</i>
V-I	C. Ignacio Rodríguez (Periférico de la Juventud – Juan Escutia)	1994
V-II	C. Juan Escutia (Av. Tecnológico – Periférico de la Juventud)	1994
V-III	C. A. de Córdoba (Av. Tecnológico – Periférico de la Juventud)	1994
V-IV	C. 38ª. (Periférico Francisco R. Almada – C. Zaragoza)	1994

The extraction procedure was performed on the basis indicated in ASTM C42 / C 42M - 04 [10] and AASHTO T 299-93 (2000) [8], and the equipment used for this purpose was a concrete core extractor machine McCulloch with 2-speed motor, 3 HP, 20 A, 120 V; 15 cm drill. For each road section three cores were obtained.

After removing each of the samples proceeded to put them in polyethylene bags properly sealed to avoid losing moisture and direct exposure to sunlight. Samples were transported to the Materials Laboratory of the Faculty of Engineering at the Autonomous University of Chihuahua. Flat surfaces were photographed using an Olympus Camera C-3040 Model 3X optical zoom and 2.5X digital zoom digital camera at a resolution of 3.3 Megapixels and analysed according to AASHTO T 299-93 [8].

3.2 Rapid Identification of Alkali – Silica Reaction Products in Concrete

Each of the 12 extracted cores was subjected to the Rapid Identification of Alkali – Silica Reaction Products in Concrete according to AASHTO T 299-93 [8]. According to this standard, the existence of brighter greenish-yellow fluorescent areas in and around coarse aggregate indicates the presence of ASR product in the sample.

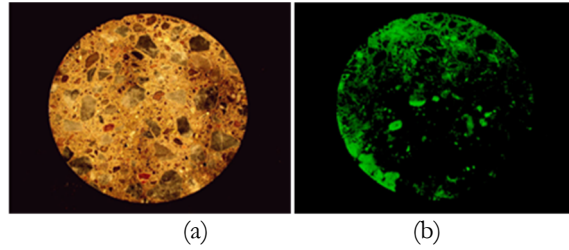


FIGURE 1: 15 cm PCCP core cut surface (Sample V-I-1): (a) This image was taken under ordinary light before the uranyl acetate solution was applied. (b) This image shows the surface under ultraviolet light after the uranyl acetate was applied.

It is important to note that some greenish-yellow fluorescent areas were discarded that may contain ASR products since the sodium in concrete reacts with uranyl acetate to form a product with the fluorescence features cited above. However, sodium is dispersed in the cement paste within the matrix of concrete but not in coarse aggregates. Also, there are carbonated uniform areas which exhibit fluorescence and that are only present in the periphery of the specimen.

3.3 Development of the Images Database

Images obtained from the process described in the previous section, were analyzed using the graphic editor GIMP 2.8. Extreme care was exercised to ensure that the photos were taken completely orthogonal to the plane of study. It is important to mention, that specific emphasis was place to match original images taken from the flat surface of the specimen with the images taken with surface treated with uranyl acetate.

In this study, ten of the twelve photographs taken of the untreated surfaces showed a mismatch; therefore they had to be adjusted using the transform tools to move, rotate, scale and perspective of GIMP 2.8. Adjustments in each are summarized in Table 2.

TABLE 2: Transformations applied to the original images.

<i>Picture of sample Id.</i>	<i>Transformation Tool Applied</i>
V-I-1	Move, scale
V-I-2	None
V-I-3	None
V-II-1	Move, Scale
V-II-2	Move, Scale
V-II-3	Move, Scale
V-III-1	Move, Scale
V-III-2	Scale
V-III-3	Move, Scale
V-IV-1	Scale
V-IV-2	Move, Scale
V-IV-3	Rotate, Scale, Move, Perspective

Once the images were adjusted and its correspondence between pairs of untreated surface and surface treated with uranyl acetate was ensure, an interest zone manual segmentation was conducted. The method consisted in delimiting areas of higher fluorescence, after identifying target areas, as shown in Figure 2.

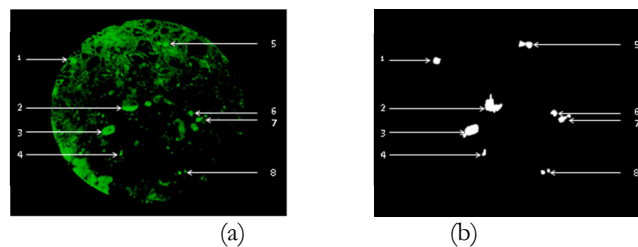
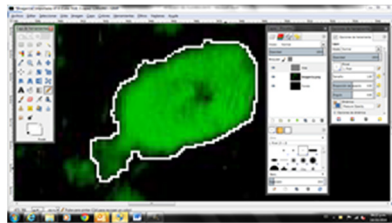


FIGURE 2: Areas of interest of sample V-I-PR1: (a) Identification of areas of interest. (b) Segmented areas of interest.

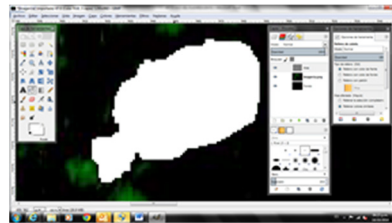
GIMP 2.8 was also used for the process of image segmentation. This method consists on obtaining areas of interest and cropping them so that individual images are generated to be used for training the computational model. The segmented areas are filled in white and the remaining areas are involved in black background. Each area, segmented and cropped, corresponds to a portion of the original photograph both untreated and treated surface. Three sets of 49 images were obtained from every image analysis.

TABLE 3: Areas of interest per picture studied.

Road	Sample	Petrography	Rapid identification AASHTO T 299-93	SEM/EDS	Images of areas of interest	Test Images
V-I	V-I-1	V-I-P1	V-I-PR1	V-I-SEM1	V-I-PR1-IMG1 a 8	V-I-PR1-IMG2 y 8
	V-I-2	V-I-P2	V-I-PR2	V-I-SEM2	V-I-PR2-IMG1 a 3	
	V-I-3	V-I-P3	V-I-PR3	V-I-SEM3	V-I-PR3-IMG1	
V-II	V-II-1	V-II-P1	V-II-PR1	V-II-SEM1	V-II-PR1-IMG1 a 6	V-II-PR1-IMG6
	V-II-2	V-II-P2	V-II-PR2	V-II-SEM2	V-II-PR2-IMG1 a 4	V-II-PR2-IMG2 y 3
	V-II-3	V-II-P3	V-II-PR3	V-II-SEM3	V-II-PR3-IMG1 a 3	
V-III	V-III-1	V-III-P1	V-III-PR1	V-III-SEM1	V-III-PR1-IMG1 a 3	V-III-PR1-IMG1
	V-III-2	V-III-P2	V-III-PR2	V-III-SEM2	V-III-PR2-IMG1 a 2	
	V-III-3	V-III-P3	V-III-PR3	V-III-SEM3	V-III-PR3-IMG1 a 5	
V-IV	V-IV-1	V-IV-P1	V-IV-PR1	V-IV-SEM1	V-IV-PR1-IMG1 a 5	V-IV-PR1-IMG3 V-IV-PR2-IMG1 y 6
	V-IV-2	V-IV-P2	V-IV-PR2	V-IV-SEM2	V-IV-PR2-IMG1 a 8	
	V-IV-3	V-IV-P3	V-IV-PR3	V-IV-SEM3	V-IV-PR3-IMG1	

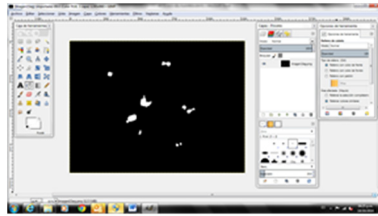


(a)

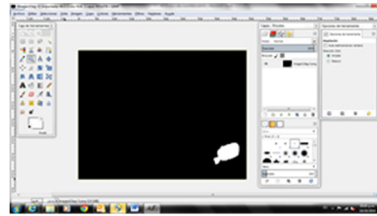


(b)

FIGURE 3: Area of interest number 3 of the Figure 2a and 2b: (a) Manual delimitation. (b) Filling the area of interest.

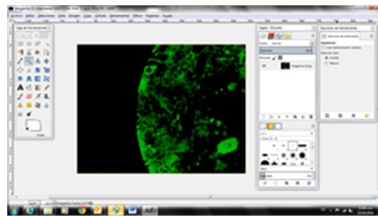


(a)

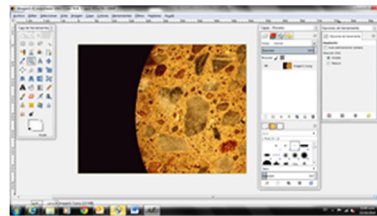


(b)

FIGURE 4: Total of segmented areas of interest (Sample V-I-PR1): (a) Equivalent to Figure 2b in GIMP 2.8 screen. (b) Cropped area of interest number 3 from Figure 2b.



(a)



(b)

FIGURE 5: Portion of sample image: (a) Corresponding to the treated image from Figure 4b. (b) Corresponding to the untreated image from Figure 4b and 5a.

3.4 Development of the Algorithm of Visual Attention (FOA).

From the work described until the previous point, the results are a bank of 49 images, in which a group of them was selected to train the Algorithm of Visual Attention (FOA). Subsequently, the algorithm

was run with images different from training images thereby detecting the same reactive zones, or very close to those initially segmented.

Currently, computational intelligence algorithms are most frequently applied in civil engineering. This computational model uses a new methodology for synthesizing programs that mimic the dorsal stream of the human visual system. It is said that human is unable to create a complete mental representation of everything in its visual field, since for processing the visual information the person should approach a region of the environment at a time. The idea behind the focus of attention is to find a part of the scene containing the prominent information to solve a particular task. In this section it will be detailed how a computational algorithm reproduces the basic phenomenon of visual attention, which is known as selectivity, which is defined as the ability to filter unwanted information [9, 13]. The FOA algorithm is based on feature integration theory, which states that visual attention is divided into two main stages: feature extraction and feature integration. Therefore, the FOA algorithm is an abstraction of the natural process which can be applied to find the location of an area of interest in the image, such as that described above.

Features extraction

In this stage the scene is perceived through a camera. The extraction of visual features is performed with a set of evolved visual operators (EVO). In this way, there will be three different EVOs, each one is specialized in the detection of a specific feature: orientation (EVO_o), color (EVO_c) and shape (EVO_s) [11, 12]. The intensity is considered as a fourth visual operator which did not evolve. Such operators can be applied on the image in a parallel way resulting in a visual map (VM) per feature dimension, see Figure 6. Thus, was proposed to use an evolutionary algorithm to discover each of these visual operators. The EVOs are used within the FOA and built based on functions and terminals presented in Table 4 and which are defined empirically as proposed in the strategy of genetic programming. Once the VM are obtained, the next step is to calculate conspicuity maps (CM), which are obtained through a center-periphery function which is applied to simulate the receptive fields in the natural vision system. The CMs are obtained according to the model proposed by Walter and Koch [14]. Finally, the CMs are combined to obtain a single saliency map as explained in the sequence.

Features integration

The next step is the fusion of the CMs into a single map of outstanding information, in order to determine the location in the visual field where attention should be directed at a given instant.

TABLE 4: Functions and terminals used for the EVOs construction.

Functions used for EVO _o
A+B, A-B, A × B, A/B, A , A+B , A-B , log(A), (A) ² , √(A), k+A, k-A, k×A, A/k, round(A), floor(A), ceil(A), inf(A,B), sup(A,B), G _{σ=1} (A), G _{σ=2} (A), D _x (A), D _y (A), thr(A)
Terminals used for EVO _o
I _r , I _g , I _b , I _c , I _m , I _y , I _k , I _s , I _v , D _x (I _s), D _{xx} (I _s), D _y (I _s), D _{yy} (I _s), D _{xy} (I _s)
Functions used for EVO _c
A+B, A-B, A × B, A/B, log(A), exp(A), (A) ² , (A) ^c , √(A), thr(A)
Terminals used for EVO _c
I _r , I _g , I _b , I _c , I _m , I _y , I _k , I _s , I _v , Op _{reg} (I), Op _{b-y} (I)
Functions used for EVO _s
A+B, A-B, A × B, A/B, k+A, k-A, k×A, A/k, round(A), floor(A), ceil(A), dilatation(A,SE _d), dilatation(A,SE _e), dilatation(A,SE _{dm}), erosion(A,SE _d), erosion(A,SE _e), erosion(A,SE _{dm}), Sk(A), Perim(A), Hit-Miss(A,SE _d), Hit-Miss(A,SE _e), Hit-Miss(A,SE _{dm}), T _{hat} (A), B _{hat} (A), opening(A,SE _s), lock(A,SE _e), thr(A)
Terminals used for EVO _s
I _r , I _g , I _b , I _c , I _m , I _y , I _k , I _s , I _v
Functions used for EFI
A+B, A-B, A × B, A/B, A , A+B , A-B , exp(A), (A) ² , √(A), round(A), floor(A), ceil(A), G _{σ=1} (A), G _{σ=2} (A), D _x (A), D _y (A)
Terminals used for EFI
CM _o , CM _c , CM _s , CM _i , D _x (CM _s), D _{xx} (CM _s), D _y (CM _s), D _{yy} (CM _s), D _{xy} (CM _s)

The saliency map (SM) defines the most prominent regions in the picture, given the characteristics of intensity, orientation, color and shape. In other words, the aim of this step is to decide where attention should be directed within the image. In this work, FOA algorithm task is to find the region of interest. Therefore, the criteria defined later must be in accordance with the purpose of the task, to guide the process towards the best combination of multiple extracted features that are built into the saliency map. Therefore, another function is evolved to integrate characteristics (EFI) which receives the information from the CM, see Figure 6. The evolutionary method uses the set of functions and terminals for EFI proposed in Table 4 to create a

fusion operator that highlights the features of the interest region. After the integration of features is performed, optimized saliency map (OSM) is obtained, which indicates the location of the most prominent region in the original image. This is known as the proto-object (Pt) measured at time t.

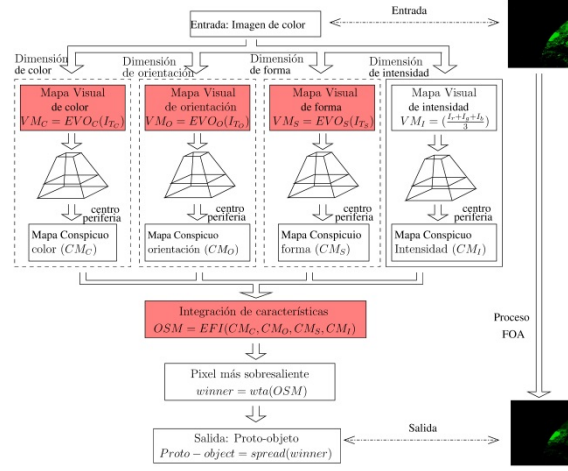


FIGURE 6: FOA Algorithm flowchart, which is applied to identify the region that corresponds to the reactive zone location in the image.

FOA Algorithm training

In this subsection the main aspects of the evolution of the FOA are explained. The explanation is divided into two steps: the training process description and definition of the fitness function.

The first stage of the evolutionary algorithm refers to the training process. At this stage the FOA learns to focus on a prominent region of the image, with the aim of characterizing the reactive zones using a reference images database. The FOA algorithm needs a flexible computational structure that allows a general solution besides a robust and simple code. In this paper was proposed that visual attention programs coded as a genotype are defined by four different operators in syntactic trees way as in the genetic programming. Three of them focus on a particular feature of the image such as color, orientation and shape, and the fourth is applied to integrate the information of the four dimensions. These trees are evolved using its own set of functions and terminals, which are independent, so that the system can be considered as a highly complex programming environment compared to classical genetic programming. Thus, each tree is initialized with a technique known as half and half, with a maximum depth of 9 levels. Given the complexity of the genotype structure there are two kinds of crossover operators and two for the mutation, which are used to vary the programming of chromosomes that create visual attention programs. Therefore, it should be understood that trees are embedded within an array.

Finally, the FOA algorithm is optimized based on the fitness of each obtained solution. Thus, the F-measure is proposed as the evaluation function between the region selected by the FOA and the location of the reactive zone. The F-measure considers both accuracy ρ and memory ϑ to determine the number of pixels that make up the intersection between the proto-object Pt and the pre-segmented region where the reactive zone is located. In this way, ρ is the number of pixels that match the two regions divided by the number of the proto-object pixels, and ϑ is the number of pixels that correspond to the intersection of the two regions divided by the number of pixels of the reactive zone. Then, the F-measure is defined as follows:

$$F\text{-measure} = 2 \times (\rho \times \vartheta) / (\rho + \vartheta) \quad (1)$$

4 RESULTS

4.1 Algorithm of Visual Attention for testing stage

Table 5 shows the results obtained by the algorithm of visual attention. Tests number 1, 6, 8 and 9, give precise results to clearly identify the segmented area of interest. Test 3 did not return any results. In the remaining tests the algorithm focused on different areas none segmented. These areas were not initially segmented, because a visual observation indicated that they were not affected by the reaction. However, it is possible that fluorescence zone detected by the algorithm is indicating the presence of gel ASR. Further testing is suggested to corroborate the assumption that ASR is present.

TABLE 5: Results of the FOA Algorithm for testing nine images.

<i>Id.</i>	<i>Treated original image</i>	<i>Segmented image overlaid to treated image</i>	<i>Zone of interest detected by the FOA algorithm</i>
V-II-PR1-IMG6			
V-II-PR1-IMG1			
V-I-PR1-IMG8			
V-II-PR2-IMG2			
V-II-PR2-IMG3			
V-IV-PR2-IMG1			
V-IV-PR1-IMG3			
V-I-PR1-IMG2			
V-IV-PR2-IMG6			

4.2 Petrographic Analysis

Petrographic examination was developed by means of sample's thin films in order to determine the presence of materials labeled as reactive. To perform the petrographic analysis it was necessary to make thin section per each of the twelve extracted cores.

A thin section is a sheet of the sample, that must have a thickness of 30 μm (0.03 mm) allowing the light to be transmitted through this fragment. Thin films preparation was performed according to ASTM C 856-04 [15].

Once the thin films were obtained, they were subjected to observation under transmitted light Olympus BX41 petrographic microscope. The summary results of petrographic analysis are shown in Table 6.

TABLE 6: Petrographic analysis results of samples.

Material	V-I-PR1-IMG2 and 8			V-II-PR1-IMG6, V-II-PR2-IMG2 and 3			V-III-PR1-IMG1			V-IV-PR1-IMG3, V-IV-PR2-IMG1 and 6		
	Coarse aggregate											
	Area (%)	Size min. (mm)	Size max. (mm)	Area (%)	Size min. (mm)	Size max. (mm)	Area (%)	Size min. (mm)	Size max. (mm)	Area (%)	Size min. (mm)	Size max. (mm)
Limestone	20.56	6.50	19.00	42.78	2.50	25.00	48.51	3.00	18.00			
Cherty limestone				4.51		12.00						
Andesite	16.55	3.00	17.00							8.43	2.00	13.00
Igimbrite/rhyolite	9.39	3.00	10.50	2.65	2.00	5.00				24.73	2.50	19.00
Basalt				1.84	3.00	6.00				9.86	4.00	12.00
Chalcedony	0.57		3.50									
Fine aggregate												
Igimbrite/rhyolite	15.88	0.10	2.48	10.85	0.18	1.56	13.56	0.21	3.36	16.55	0.18	3.52
Quartz	3.30	0.04	2.15	3.05	0.12	1.07	2.57	0.08	1.11	2.03	0.08	0.98
Andesite	1.59	0.27	3.22	2.09	0.51	1.37	1.07	0.35	0.98			
Feldspar	1.44	0.10	0.68	1.97	0.12	0.98	2.75	0.10	1.05	0.75	0.16	0.43
Limestone	0.88	0.04	1.56	1.33	0.98	1.50	0.39	0.12	1.17			
Strained Quartz	0.47	0.29	0.72	1.57	0.23	1.27	0.86	0.12	0.53	1.28	0.23	2.00
Opal	0.40	0.02	0.20	0.44	0.20	0.23	0.51	0.04	0.23	0.49	0.01	0.29
Granite	0.29		0.82							0.43	0.72	1.02
Chalcedony	0.18	0.16	0.62	0.88	0.23	0.98	0.64	0.66	1.07	1.94	0.23	2.34
Fiber	0.11	0.10	0.55	0.44	0.14	1.17	0.06	0.14	0.39	0.33	0.20	3.90
Basalt				0.40	0.29	0.59	1.72	0.31	0.86	0.28	0.43	1.92
Pyroxene				0.04		0.16	0.04		0.25			
Biotite							0.04		0.23			
Hematite										0.04		0.12
Lithic fragment chloritized										1.70		2.93
Voids	2.50	0.20	0.98	1.93	0.98	1.76	1.37	0.20	1.21	1.47	0.12	1.17
Matrix	25.89			23.23			25.91			29.69		
Total	100.0			100.0			100.0			100.0		

4.3 Scanning Electron Microscope Analysis

EDS analysis was held in a powder sample extracted from area showed in Figure 7. The equipment used was a JEOL model JSM-5800LV microscopy coupled with EDS analyzer EDAX model DX prime. The results of its elemental composition are shown in Table 7. The picture was taken by optical microscopy at 20x. The morphology of the ASR gel can be observed in Figure 7.

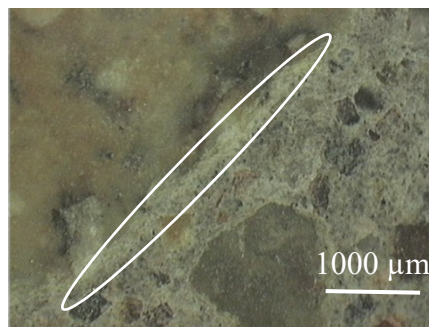


FIGURE 7: Selected area of Sample V-I-SEM2

TABLE 7: Results of deposited material in cracks of the sample V-I-SEM2.

<i>Element</i>	<i>Wt%</i>	<i>At%</i>
C K	10.93	17.75
O K	41.95	50.54
Na K	2.94	2.50
Mg K	0.53	0.42
Al K	8.12	5.87
Si K	26.65	18.51
P K	0.29	0.18
S K	0.26	0.16
K K	5.06	2.52
Ca K	1.70	0.83
Fe K	2.07	0.72
TOTAL	100.00	100.00

Table 8 shows a summary of results of all laboratory tests; they corroborate the ASR gel product also detected by the algorithm.

From the results obtained in validation tests, it can be concluded the potentiality of the FOA to detect the presence of ASR based on concrete samples treated with uranyl acetate.

TABLE 8: Laboratory test results of Portland cement concrete samples.

<i>Sample</i>	<i>Petrographic Analysis (potentially reactive material %) (ASTM C 856 – 04)</i>	<i>Rapid Identification of Alkali-Silica Reaction Products in Concrete AASTHO T299-93 (2000)</i>	<i>Analysis of material deposited in cracks (present in At%):</i>
V-I-1	Chalcedony 0.75	Green fluorescence was observed in the coarse aggregate and cementitious matrix; ASR presence.	Si 2.35
V-I-2	Andesite 18.14 Rhyolite 25.27		Na 0.53 K 0.44
V-I-3	It was not carried out	Green fluorescence was observed in the coarse aggregate and cementitious matrix; ASR presence.	Si 18.51 Na 2.50 K 2.52
V-II-1	Chalcedony 0.88	Green fluorescence was observed in the coarse aggregate and cementitious matrix; ASR presence.	Si 8.03
V-II-2	Andesite 2.09 Rhyolite 13.50		Na 1.07 K 0.88
V-II-3	It was not carried out	Green fluorescence was observed in the coarse aggregate and cementitious matrix; ASR presence.	Si 12.96 Na 1.63 K 1.09
V-III-1	Chalcedony 0.64	Green fluorescence was observed in the coarse aggregate and cementitious matrix; ASR presence.	Si 11.57
V-III-2	Andesite 1.07 Rhyolite 13.56		Na 1.32 K 1.03
V-III-3	The same average as T1-10-1	Green-yellow area, the presence of ASR gel is observed in aggregate	Si 6.11 Na 1.05 K 0.51
V-IV-1	Chalcedony 1.94	Green fluorescence was observed in the coarse aggregate and cementitious matrix; ASR presence.	Si 6.42
V-IV-2	Andesite 8.43 Rhyolite 41.28		Na 0.73 K 0.43
V-IV-3	It was not carried out	Low occurrence of greenish fluorescence is observed in aggregates and matrix; ASR presence	Si 6.75 Na 0.73 K 0.50
		Green fluorescence was observed in the coarse aggregate and cementitious matrix; ASR presence.	Si 3.01 Na 0.05 K 0.30
		Green-yellow areas were observed; ASR presence	Si 11.35 Na 1.00 K 0.90
		Green-yellow areas were observed; ASR presence	Si 15.40 Na 1.30 K 1.14
		Green fluorescence was observed in the coarse aggregate and cementitious matrix; ASR presence.	Si 23.82 Na 2.20 K 2.14

5 DISCUSSION

This paper uses a new methodology for synthesizing that mimic the dorsal stream of the human visual attention FOA algorithm, in order to detect reactive zones in concrete deteriorated by ASR. There are not precedents in literature about this.

It is important to note that the criterion for segmentation of areas of interest from deteriorated concrete treated with uranyl acetate was visual observation. The brighter greenish-yellow fluorescent zones are indicative of presence of ASR product gel according to AASHTO T 299-93 [8].

The results of FOA algorithm for testing images were successful to identify previously segmented areas in 44.4% of cases. FOA algorithm gave no results in 11.1% of cases. FOA algorithm failed to identify previously segmented areas in 44.4% of cases.

Petrographic examination of PCCP cores samples was used to identify reactive aggregates. SEM/EDS analysis was used to identify the presence of ASR product gel. It was found that in all images (i.e. 100%) was detected the presence of reactive minerals and the material deposited in cracks was the ASR product gel. Therefore, it is possible that in the cases of test images: 2, 4, 5 and 7, the areas of interest detected by FOA were reactive. Further petrographic examination is necessary in order to corroborate this assumption.

A greater number of images are necessary to improve the training efficiency of the FOA algorithm. Computational vision techniques can be effective to accurately detect reactive zones in deteriorated concrete by ASR.

6 CONCLUSIONS

The visual detection techniques applied to concrete images treated with uranyl acetate proved to be potentially effective for detecting ASR product gel. Petrographic and SEM analysis were used to validate the results of FOA algorithm. Visual attention algorithm (FOA), developed in this work for detecting ASR product gel, could be used to facilitate inspecting and monitoring damaged structures by ASR.

7 REFERENCES

- [1] Stark, D (1991): Handbook for the Identification of Alkali-Silica Reactivity in Highway Structures SHRP-C-315. Strategic Highway Research Program. National Research Council, Washington, D. C.: pp 50.
- [2] ACI (1998): State-of-the-Art Report on Alkali-Aggregate Reactivity. ACI 221.1R-98. American Concrete Institute: pp 30.
- [3] FHWA (2011): Alkali – Silica Reactivity Field Investigation Handbook. Report No. FHWA-HIF-12-022. Federal Highway Administration: pp 80.
- [4] FHWA (2013): Alkali-Aggregate Reactivity (AAR) Facts Book. Report No. FHWA-HIF-13-019. Federal Highway Administration: pp 224.
- [5] García del Amo, D, and Calvo, B (2001). Diagnosis of the Alkali-silica reactivity potential by means of digital image analysis of aggregate thin sections. *Cement and Concrete Research* (31): 1449-1454.
- [6] Castro, N, and Wigum, BJ (2012): Assessment of the potential alkali-reactivity of aggregates for concrete by image analysis petrography. *Cement and Concrete Research* (42): 1635-1644.
- [7] Špařtná, A, Šachlová, Š, Pertold, Z, Pírkryl, R, and Leichmann, J (2012): Cathodoluminescence microscopy and petrographic image analysis of aggregates in concrete pavements affected by alkali-silica reaction. *Materials Characterization* (65): 115-125.
- [8] AASHTO T 299-93 (2000): Rapid Identification of Alkali – Silica Reaction Products in Concrete Standard Specifications for Transportation Materials and Methods of Sampling and Testing, Part 2 – Tests. American Association of State Highway and Transportation Materials, T299-1 – T299-6.
- [9] Desimone, R, and Duncan, J (1995): Neural mechanisms of selective visual attention. *Annual Reviews* (18): 193-222.
- [10] ASTM C42/C 42M – (2004): Standard Test Method for Obtaining and Testing Drilled Cores and Sawed Beams of Concrete, Annual Book of ASTM Standards, Section Four Construction, Volume 04.02 Concrete and Aggregates, 31 – 36.
- [11] Treisman AM, and Gelade G. (1980): A feature-integration theory of attention. *Cogn Psychol*; 12: 97-136.
- [12] Dozal, LF, Olague, G, Clemente, E, and Hernández, ED (2014): Brain Programming for the Evolution of an Artificial Dorsal Stream. *Cognitive Computation* (6): 528-557.
- [13] Clemente, E, Chavez, F, Fernández, F, and Olague, G (2014): Self-Adjusting Focus of Attention in Combination with a Genetic Fuzzy System for Improving a Laser Environment Control Device System. *Applied Soft Computing* (32): 250-265.
- [14] Walther, D, and Koch, C (2006): Modeling attention to salient proto-objects. *Neural Networks* (19): 1395-407.
- [15] ASTM C856–04 (2004): Standard Practice for Petrographic Examination of Hardened Concrete. American Society for Testing & Materials, Annual Book of ASTM Standards (Lakušić & Ahac, 2012)(04.02): Section Four Construction, Concrete and Aggregates: 438 – 454.